A New State Space Model for the NASA/JPL 70-Meter Antenna Servo Controls

R. E. Hill
Ground Antenna and Facilities Engineering Section

A control axis referenced model of the NASA/JPL 70-m antenna structure is combined with the dynamic equations of the servo components to produce a comprehensive state variable (matrix) model of the coupled system. An interactive Fortran program for generating the linear system model and computing its salient parameters is described. Results are produced in a state variable, block diagram, and in factored transfer function forms to facilitate design and analysis by classical as well as modern control methods.

I. Introduction

The upgrade of the NASA/JPL 64-m antennas to 70-m apertures has added considerable mass and inertia moment on top of the existing alidade with resultant decreases in the natural frequencies of the structure. Because the combined compliances of the alidade and gear reducers separate the autocollimator from the antenna servo motors and tachometers, the increased inertia can affect the dynamics of autocollimator based pointing control. A study was undertaken to assess the impact on the axis servos of the increased inertia and decreased frequencies and to provide a more complete model for the new servo design. This article describes the methodology of combining the dynamics of the structure with those of the servo and cites results for both the 64-m and 70-m antennas.

The development of a condensed antenna structural model [1] provides a control axis referenced representation of the structure dynamics in a compact form. When integrated with the dynamic properties of the hydraulic actuators and the control electronics, the result is a more comprehensive model for design, analysis, and simulation of the axis servos. The composite model is derived by coupling the linear differential equations describing the structure with those of the control components to produce a state variable model.

The structure model consists of a relatively large residual inertia to which are coupled individual modal inertias. For the elevation axis, two modes of the alidade structure are added. The elasticity of the control actuators, the compliance and inertia of the hydraulic system, the drive motors, and the characteristics of the servo compensation networks are also superimposed. In the most inclusive of the optional forms available, the elevation model representing five modal inertias and two alidade modes results in a nineteenth order linear system model.

The antenna pointing system employs two modes of position feedback derived from either a shaft angle encoder driven through a precision gear reducer from the bullgear, or an optical autocollimator mounted at the rear of the apex of the main reflector. The autocollimator mirror is attached to an hour

angle-declination mount on a pedestal isolated from that of the antenna. The structure model includes the transformation coefficients relating the displacement at the autocollimator reference structure to the arbitrary coordinates of the individual inertias. These coefficients enable system modeling of displacements at the autocollimator as well as at the encoder and tachometers, all of which are connected by nonzero flexibilities.

The state variable representation has one limitation in that system response properties are not evident by inspection when large system matrices are involved. For example, the existence of a pole in the right-half s plane, evident in a root locus display, is not recognizable by inspection of a linear system matrix unless the matrix happens to be in a form where the eigenvalues are recognizable. The matrix form of system representation does, however, provide great flexibility to accommodate various computer processing methods. Thus, both transfer function and block diagram representations are readily derived from the open loop as well as the closed rate loop system matrices. The results are available in a variety of forms suitable for classical as well as modern control system design and analysis.

An interactive Fortran program was developed for generating the model in state variable (matrix) form. Operating on an IBM PC, the program provides options for adjustment of the complexity of the model and of various parameter values. It displays the resultant linear system matrix and computes the corresponding system poles from the eigenvalues of the system matrix. Zeros of each of the tachometer, encoder, and autocollimator responses are determined from the eigenvalues of partitioned matrices formed according to the Mason gain formula [2]. Zeros of the autocollimator response are computed from the weighted sum of encoder and individual mode zeros where the weighting factors are the transformation coefficients mentioned earlier. This indirect method was used as an expedient to avoid coding an algorithm for the more general solution of zeros of the transformed matrix.

II. Structure Dynamics Model

The form of the condensed structure mode for the elevation axis is shown schematically in Fig. 1. In Fig. 1 θ_{A1}, θ_M, and θ_B correspond, respectively, to the angular rates of motion at the gear reducer attachment, the reducer output pinion (normalized with respect to the pinion to bullgear ratio), and the twin bullgears. The combined stiffness of the four gear reducers (two driving each bullgear) is represented by a single spring, K_G, shown connected between the pinion and the "single" bullgear. The angular rates of the individual modal inertias θ_1 through θ_N have an indirect correspondence to the motion of the physical antenna. A set of dimensionless coefficients, alpha, relate the motion of the Intermediate Reference Structure to θ_1 through θ_N.

While the azimuth axis of the antenna employs a single, stationary bullgear and moving gear reducers, its dynamic motion can be described using the same model as in the elevation axis. A small error results, however, because in azimuth, the reducer housing rotates with the alidade, such that in 360 degrees of azimuth motion each azimuth drive motor shaft makes $N-1$ revolutions relative to the pedestal and only N revolutions relative to the alidade. The error arises because the motor torque-speed characteristic is referenced to alidade coordinates, while acceleration torque is proportional to motion in inertial coordinates. However, since the gear ratio, N, is large, the resulting error is negligible.

Using the coordinate definitions of Fig. 1, the equations of motion for the individual inertias, J_i, are derived. In general, a small damping, D_i, is associated with each spring, K_i.

$$J_i\ddot{\theta}_i + D_i(\dot{\theta}_i - \dot{\theta}_B) + K_i(\theta_i - \theta_B) = 0 \qquad \text{for } i = 1 \text{ to } N \tag{1}$$

$$J_B\ddot{\theta}_B + (K_G + \sum_1^N K_i)\theta_B - \sum_1^N (D_i(\dot{\theta}_i - \dot{\theta}_B) + K_i\theta_i) = K_G\theta_M \tag{2}$$

$$J_{A1}\ddot{\theta}_{A1} + K_{A1}\theta_{A1} - K_{A1}\theta_{A2} + K_G(\theta_M - \theta_B) = 0 \tag{3}$$

$$J_{A2}\ddot{\theta}_{A2} + (K_{A1} + K_{A2})\theta_{A2} - K_{A1}\theta_{A1} = 0 \tag{4}$$

III. Hydraulic Motor Model

A schematic representation of the hydraulic system and gear reducers is shown in Fig. 2. Each gear reducer includes two fixed displacement, axial piston hydraulic motors driving a spur gear reducer. One motor provides control and the other produces a constant value countertorque. The countertorque motors are coupled to a regulated hydraulic pressure supply and connected so as to produce opposite torque outputs from two of the four reducers. This arrangement eliminates backlash in all gear meshes except the single mesh between each control motor and the first intermediate gear. The countertorque has the added benefit of increasing the incremental torque stiffness of the reducer geartrains. Control motor modulation is provided by a four-port hydraulic servovalve interconnecting a regulated high pressure hydraulic source and return with the motors.

The dynamic model of the drive motors and hydraulic system is derived according to established practices. Because the high gain of the rate servo loop diminishes the overall effects of friction, leakage, and valve pressure variations, a comparatively simple, second order, linearized model can be justified. Neglecting leakage, the oil flow, Q_m, through the hydraulic motor is given by

$$Q_m = V \dot{\theta}_m$$

where V is the volumetric displacement of the motor and $\dot{\theta}_m$ is the rotational speed at the output shaft.

Equating the fluid input power and the mechanical output power yields the relationship between motor torque, T_m, and hydraulic pressure, P

$$T_m = PV$$

The oil flow through the hydraulic servo valve is described by the equation of flow through a sharp edge orifice of variable size

$$Q_v = K_v I_v P_v^{1/2} \tag{5}$$

where P_v is the pressure drop across the valve, K_v is the flow constant of the valve, and I_v is the valve coil current.

The valve pressure drop equals the pressure difference between the regulated supply and the motor. Since both analytic and field test results show the steady state pressure drop is relatively constant in the range of 2000 to 2500 psi (13790 to 17238 kPa), a piecewise linear approximation of the above orifice equation is sufficient. Transient pressure drops caused by large acceleration or high wind torque will effectively decrease the rate loop gain and increase valve damping relative to the values represented by the linear approximation. With the aid of a root locus diagram, it can be shown that the net effect on the rate loop stability is negligible.

The linearized valve equation combined with the motor and compressible flow equations is illustrated in block diagram form in Fig. 3 where C and J_m represent the hydraulic compliance and motor inertia, respectively. The valve gain and damping constants K_p and D, respectively, are derived by partial differentiation of the valve flow Eq. (5) with values of P_v and Q_v that represent mean operating conditions. The damping parameter D may be increased to include motor leakage and other equivalent sources of damping.

In rearranging the above equations to a form compatible with the structure equations, a provision for the motion of the flexible structure supporting the reducer is required. This is accomplished by equating the motor rotation to the difference between θ_m and θ_{A1} in Fig. 1. Thus by application of the Mason gain rule to the diagram of Fig. 3 and with the definition of the reducer natural frequency

$$\omega_m = \left(\frac{V^2}{J_m C}\right)^{1/2}$$

the gear reducer equation is obtained as:

$$N_r \left(s^2 + \frac{D}{C} s + \omega_m^2\right)(\dot{\theta}_m - \dot{\theta}_A) + \frac{T_x}{N_r J_m}\left(s + \frac{D}{C}\right) = \frac{Q}{V}\omega_m^2 \tag{6}$$

where $Q = K_p I_v$ is the effective no-load valve flow and N_r is the overall motor-to-axis gear ratio.

The large value of gear ratio N_r (28700) permits the omission of the acceleration torque term that arises from the difference between reducer and inertial coordinates, with a small error resulting.

IV. System Equations

Equating the reducer shaft torque, T_x, to the torque transmitted by the reducer stiffness, K_G completes the equations defining the coupled actuation-structure system as follows:

$$T_x = K_G(\theta_m - \theta_B) \tag{7}$$

To accommodate analyses of the servo rate loops as well as the position loops, and also to facilitate computation of transfer function parameters, the system equations are developed in two steps. First, the open loop linear system matrix and associated input and output vectors are derived from Eqs. (1) through (7) above. Subsequently, the closed loop system matrix is formed by augmentation of the open loop matrix by inclusion of the rate feedback and compensation gains. The system state equations are derived from Eqs. (1) through (7) above using the state variable definitions in Table 1. The variable definitions are generalized to accommodate either the azimuth or elevation axis and a variable number of structure modes, N. Because the azimuth structure model is based upon the assumption of a rigid pedestal, state variables corresponding to $\dot{\theta}_{A1}$ and $\dot{\theta}_{A2}$ are absent from the azimuth model.

It will be seen that with the exception of the third, $(2N+5)$th, and $(2N+9)$th variables, all rates and accelerations are relative to stationary coordinates. The third variable corresponds to the effective rotor-stator rotation of the hydraulic motor and of the tachometer. The $(2N+5)$ and $(2N+9)$ variables corre-

spond to the effective extension of the gear reducer torsional stiffness for the azimuth/elevation axes, respectively. This torsional extension is related to the reducer output torque through the stiffness parameter K_G.

The resulting state equations for the elevation axis are listed in generalized form in Table 2. Using

$$\dot{\mathbf{X}} = [F]X + [G]U \tag{8a}$$

$$\mathbf{Y} = [H]X \tag{8b}$$

with $\mathbf{X}$ the state vector, $\dot{X}$ the time derivative of $\mathbf{X}$, U the system input, and Y the output, the corresponding linear system matrices are listed in Table 3. The system block diagram is shown in Fig. 4. The azimuth equations, matrices, and block diagram are similar to their elevation counterparts, except the four alidade states are omitted.

V. Derivation of Transfer Functions

The linear transfer functions relating the inputs and outputs are expressed as ratios of factored polynomials in the Laplace operator, s. The respective numerator and denominator factors are of the form (s – zero) and (s – pole) and are related to the system matrices through the traditional equations expressing the conditions for the poles and zeros of the response.

For system poles (denominator factors):

$$[sI - F] = [0] \tag{9}$$

For system zeros (numerator factors):

$$\begin{bmatrix} (sI - F) & -G \\ H & 0 \end{bmatrix} \begin{bmatrix} X(s) \\ U(s) \end{bmatrix} = [0] \tag{10a}$$

Equation (9) is an eigenvalue equation and the system poles are the eigenvalues of the linear system matrix. Software for eigenvalue evaluation is available for DOS microcomputers. For the more complicated case of Eq. (10) for evaluating the zeros, a more convenient method based on the Mason gain rule was employed. An advantage of this alternate method is that it reduces the dimensions of the matrices to be processed, thus improving numerical accuracy.

The method is based upon an adaptation of Mason's [2] signal flow graph gain (transfer function) determination, to state variable representations. Mason relates transfer function denominator and numerator to "determinants" of flow graphs and of certain subgraphs. It can be shown that these determinants of flow graphs are identical to the determinants of corresponding matrices representing the equations of the graphs. Using this equivalence, the transfer function numerator thus becomes the determinant of the partitioned matrix formed by deleting from the system equations those state variables included along the forward path in a flow graph representation of the equations. Since forward paths are recognizable in system equations, this partitioning can be accomplished without actually constructing the graph. The numerator factors are thus determined from the eigenvalues of the partitioned matrix formed above.

The zeros for the autocollimator and elevation encoder output responses are computed by superposition of individual components of the respective responses. This superposition avoids both a coordinate transformation of the system matrix and also the relatively complicated application of the Mason rule to a transformed matrix. Because it involves weighted summations of characteristic polynomials with subsequent factoring, this method is subject to numerical inaccuracy as matrix size increases. Good accuracy has resulted for models including three structure modes. The accuracy of this method could be improved and its usefulness extended to more modes by frequency scaling in such a way as to reduce the numeric range of the polynomials. Using superposition, the general case for the encoder response characteristic polynomial, P_E, is given by

$$P_E = \frac{K_G}{J_B} P_B - \frac{K_G}{J_{A1}} P_A \tag{10b}$$

where the response zeros are the roots of P_E; P_B and P_A are the characteristic polynomials of the bullgear and alidade responses, respectively. They are the characteristic polynomials of submatrices formed according to the method described above. Equation (10b) can be applied to the azimuth axis by equating P_A to zero.

The complexity of the elevation autocollimator response is reduced by partitioning into two smaller systems with the results combined so as to avoid processing polynomials of high order. The validity of this simplification is evident from the bullgear response submatrix formed by deleting the state variables included in the forward path between input and the bullgear rate. This submatrix is formed from the **F** matrix of Table 3 by deletion of rows and columns 1 through 4. Since this submatrix consists of two diagonal blocks, with one block representing the alidade and the other representing the tipping structure, the eigenvalues are simply the combination of those of the individual blocks. The complete solution of the autocollimator response is the weighted superposition of the responses of the bullgear and of the individual inertias, all of which are derived from this block diagonal matrix. The zeros of the

autocollimator response are thus the roots of characteristic polynomial P_{AC} defined by Eqs. (10c) and (10d):

$$P_{AC} = (P_A)\left(a_0 P_{BB} + \sum_1^N a_i \omega_i^2 P_i\right) \tag{10c}$$

$$\mathbf{F_B} = \begin{bmatrix} \mathbf{F}_{BB} & 0 \\ 0 & \mathbf{F}_A \end{bmatrix} \tag{10d}$$

where polynomials P are derived from their corresponding $\mathbf{F}$ matrices having the same subscripts, $\mathbf{F}_B$ is the bullgear response submatrix described above, and the $\mathbf{F}_i$ matrices are derived from $\mathbf{F}_{BB}$ by row, column deletion by the aforementioned principle. Coefficients $a_0 \cdots a_N$ in Eq. (10c) are the transformation coefficients provided in the structure model.

The physical significance of this partitioning is explained by considering the individual uncoupled responses of the alidade and the tipping structure to a torque input applied at the elevation gear reducer. The frequencies of infinite compliance (i.e., zero stiffness) of the alidade are frequencies of bullgear response zeros and are not influenced by the tipping structure. Additional frequencies of zero bullgear response are the natural frequencies of the individual tipping structure modes and are not influenced by the presence of the alidade. The partitioning is thus valid and no loss of generality results from its use.

VI. Closed Rate Loop Model

Modeling of the closed rate loop configuration is accomplished by extending the open loop equations and matrices to include the rate feedback and loop compensation. In both the 64-m and 70-m rate loops, tachometer based feedback, a lag/lead network, and a lead/lag network are employed to obtain a high degree of stiffness at low frequency and a comparatively narrow noise bandwidth. Since the 50 Hz servovalve bandwidth is sufficiently wide to have negligible effect on loop dynamics, the rate feedback can be modeled by the two phase compensation networks and a gain parameter.

The transfer function of the tachometer-network-amplifier, servovalve cascade is:

$$\frac{Q(s)}{\dot{\theta}_M(s)} = \frac{K_r V}{\omega_m^2} \frac{(s+Z_1)}{(s+P_1)} \frac{(s+Z_2)}{(s+P_2)} \tag{11}$$

The two real poles of Eq. (11) result in two additional states with the following additional state equations:

$$\dot{x}_M = -K_r(Z_1 - P_1)x_3 - P_1 x_M \tag{12}$$

$$\dot{x}_{M+1} = -K_r(Z_2 - P_2)x_3 + (Z_2 - P_2)x_M - P_2 x_{M+1} \tag{13}$$

where

$M = 2N+6$ for azimuth and
$M = 2N+10$ for elevation

For the closed loop case the equation for $\dot{x}_4$ becomes

$$\dot{x}_4 = -(\omega_m^2 + K_r)x_3 - \frac{D}{C} x_4 + x_m + x_{m+1} \tag{14}$$

The closed rate loop linear system matrix is obtained by augmenting the open loop matrix of Table 3 according to Eqs. (12), (13), and (14) and is shown in Table 4.

The various transfer functions for the open and closed loop systems are compiled according to the following properties of linear systems:

(1) all transfer functions in a given system have identical poles.

(2) the zeros in any given transfer function are invariant with respect to gain changes in other parts of the system not touching the forward path under consideration.

Property (1) implies that the tachometer, encoder, and autocollimator transfer functions all have identical poles, thus eliminating a need for repeated computations. Because the loop closing gain is in a feedback path, property (2) allows the use of zeros computed for the open loop case in the closed loop transfer functions. The real zero at –2.2, appearing in the closed loop functions, results from an electronic compensation network in the forward path.

VII. Numerical Results

A generalized Fortran program for generating the linear system matrix and computing the corresponding poles and zeros was developed and executed on an IBM PC. The program provides options for selection of axis, display and adjustment of parameter values, and adjustment of the number of structure modes included. As the number of modes is adjusted downward, the inertia of the rejected modes is added to the residual inertia, thus maintaining accuracy of the total inertia. Results are written to disk-files in a format compatible with postprocessing programs.

The Fortran program was used to derive models for the azimuth and elevation axes of both 64-m and 70-m configurations. Hardware parameter values available for the four configurations are listed in Table 5. In some cases the number of structure modes modeled was reduced from the number available in order to reduce computation and data space. For the 64-m azimuth case the 4th mode was eliminated, for 70-m azimuth the 5th mode was eliminated, and for 70-m elevation the 3rd, 4th, and 5th modes were merged into a weighted composite. The best estimate of structure damping ratio available is 0.003, which was observed in factory tests of the 70-m quadripod. Because of computation error in some of the zeros computations resulting from nonzero damping, all computations were run with zero structure damping. The introduction of appropriate damping would displace the complex zeros from the imaginary axis and cause a similar displacement of the complex poles. However, since the poles are already damped by the rate loop, the introduction of structure damping would have small effect on the overall results.

The poles and zeros of the open and closed rate loop transfer functions are listed in Table 6. In cases where inertia values other than those of Table 5 were used, the actual values are included in Table 6. Frequency response plots of amplitude vs. radian frequency for the 70-m azimuth and elevation axes are shown in Figs. 5 and 6.

The differences between the tachometer, encoder, and autocollimator responses are due to the flexibility of the gear reducers and structure between the respective devices. In the elevation autocollimator responses, the low frequency (2 Hz for 64-m, 1.5 Hz for 70-m) resonant peak and subsequent roll-off result from the flexibility of the alidade. It occurs because alidade deflections in elevation are sensed by the autocollimator but not by the encoder. Both the encoder and autocollimator responses for both 64-m axes show a high frequency roll-off beginning at 6.7 to 7.2 Hz. For the 70-m configuration the roll-off frequencies are nearly identical, 6.5 to 6.8 Hz. This result is explained by the fact that most of the inertia increase resulting from the upgrade is associated with the first three modes while the residual inertias are relatively unchanged.

VIII. Conclusions

The models described have enabled the design of the rate and position servos for the 70-m configuration with a minimum of on-site adjustment. The azimuth axis structure model, see Table 5, includes three low frequency modes at 1.27 to 1.42 Hz, a frequency roughly half that of the lowest mode in the 64-m configuration. These modes are a cause for concern because of their low frequencies, close spacing, and relatively large associated inertias which make damping by the servo loop difficult to achieve. The presence of these modes necessitated an increase of the motor shaft mounted inertia wheels as a means of diminishing their effect on the control system.

The results summarized in Table 6 provide improved definition of the encoder and autocollimator response characteristics as compared with those based on the assumption of a "rigid" alidade structure. These results will be useful in future efforts to improve autocollimator based pointing. They do not necessitate immediate changes as a result of the upgrade.

References

[1] R. Levy, "Condensed Antenna Structural Models for Dynamic Analysis," *TDA Progress Report 42-80*, vol. October–December 1984, Jet Propulsion Laboratory, Pasadena, California, pp. 40–61, February 15, 1985.

[2] S. J. Mason, "Feedback Theory-Further Properties of Signal Flow Graphs," *Proc. IRE*, vol. 44, pp. 920–926, July 1956.

Table 1. State variable definitions

Variable	Symbol	Description
x_1	$\dot{\theta}_B$	Bullgear angular rate
x_2	$\dot{x}_1$	Bullgear acceleration
x_3	$\dot{\theta}_M - \dot{\theta}_{A1}$	Motor/tach rate
x_4		Hydraulic torque/J_m
x_{2i+3}	$\dot{\theta}_i$	Angular rate at the inertia J_i for i = 1 to N
x_{2i+4}	$\dot{x}_{2i+3}$	
x_{2N+5}	$\theta_M - \theta_B$	Motor–bullgear angle difference, azimuth only
x_{2N+5}	$\dot{\theta}_{A1}$	Angular rate at alidade 1, elevation only
x_{2N+6}	$\dot{x}_{2N+5}$	Elevation only
x_{2N+7}	$\dot{\theta}_{A2}$	Angular rate at alidade 2, elevation only
x_{2N+8}	$\dot{x}_{2N+7}$	Elevation only
x_{2N+9}	$\theta_M - \theta_B$	Motor–bullgear angle difference, elevation only

Table 2. State equations for elevation

$$\dot{x}_1 = x_2$$

$$\dot{x}_2 = -\left(\frac{K_G}{J_B} + \sum_1^N \frac{K_i}{J_B}\right) x_1 + \sum_1^N \frac{K_i}{J_i} x_{2i+3} + \frac{K_G}{J_B} x_3 + \frac{K_G}{J_B} x_{2N+5}$$

$$\dot{x}_3 = x_4 - \frac{K_G}{J_M} x_{2N+9}$$

$$\dot{x}_4 = -\omega_m^2 x_3 - \frac{D}{C} x_4 + \frac{Q}{V} \omega_m^2$$

$$\dot{x}_{2i+3} = x_{2i+4} \qquad \text{for } i = 1 \text{ to } N$$

$$\dot{x}_{2i+4} = \omega_i^2 x_i \neq \frac{D_i}{J_i} x_2 - \omega_i^2 x_{2i+3} - \frac{D_i}{J_i} x_{2i+4}$$

$$\dot{x}_{2N+5} = x_{2N+6}$$

$$\dot{x}_{2N+6} = \frac{K_G}{J_{A1}} x_1 - \frac{K_G}{J_{A1}} x_3 - \frac{K_G + K_{A1}}{J_{A1}} x_{2N+5} + \frac{K_{A1}}{J_{A1}} x_{2N+7}$$

$$\dot{x}_{2N+7} = x_{2N+8}$$

$$\dot{x}_{2N+8} = \frac{K_{A1}}{J_{A2}} x_{2N+5} - \frac{K_{A1} + K_{A2}}{J_{A2}} x_{2N+7}$$

$$\dot{x}_{2N+9} = -x_1 + x_3 + x_{2N+5}$$

N = number of structure modes in model

Table 3. Linear system matrices for open loop elevation axis

$$
\mathbf{F} = \begin{bmatrix}
0 & 1 & & & & & & & & & & & & & & & 0 \\
\frac{-K_G - K_T}{J_B} & 0 & \frac{K_G}{J_B} & 0 & \frac{K_1}{J_1} & 0 & 0 & 0 & 0 & 0 & 0 & \frac{K_G}{J_B} & & & & & 0 \\
 & & 0 & 1 & & & & & & & & & & & & & \frac{-K_G}{J_M} \\
 & & -\omega_m^2 & \frac{-D}{C} & & & & & & & & & & & & & \\
 & & & 1 & 0 & & & & & & & & & & & & \\
\omega_1^2 & \frac{D_1}{J_1} & & & -\omega_1^2 & \frac{-D_1}{J_1} & & & & & & & & & & & \\
 & & & & & & & 0 & & & & & & & & & \\
 & & & & & & & & 1 & 0 & & & & & & & \\
\omega_N^2 & \frac{D_N}{J_N} & & & & & & & & -\omega_N^2 & \frac{-D_N}{J_N} & & & & & & \\
 & & & & & & & & & & & 0 & 1 & & & & \\
\frac{K_G}{J_{A1}} & 0 & \frac{-K_G}{J_{A1}} & 0 & 0 & 0 & 0 & 0 & 0 & 0 & 0 & -\frac{K_G + K_{A1}}{J_{A1}} & 0 & \frac{K_{A1}}{J_{A1}} & & & \\
 & & & & & & & & & & & & & 0 & 1 & & \\
 & & & & & & & & & & & \frac{K_{A1}}{J_{A2}} & 0 & -\frac{K_{A1} + K_{A2}}{J_{A2}} & 0 & & \\
-1 & 0 & 1 & 0 & 0 & 0 & 0 & & 0 & 0 & 0 & 1 & 0 & & & & 0
\end{bmatrix}
$$

Note: $K_T = \sum_1^N K_i$

LINEAR SYSTEM INPUT MATRIX, **G**

$$
\mathbf{G} = \left(\frac{\omega_m^2}{\mathrm{V}}\right) \begin{bmatrix} 0 \\ 0 \\ 0 \\ 1 \\ 0 \\ \cdot \\ \cdot \\ \cdot \\ \cdot \end{bmatrix}
$$

Table 3. (contd)

OUTPUT VECTORS, **H**

FOR TACHOMETER OUTPUT RESPONSE

$\mathbf{H_T}$ = [0 0 1 0 ..... 0]

FOR ENCODER OUTPUT RESPONSE

$\mathbf{H_{Ea}}$ = [1 0 0 0 ..... 0] Azimuth only

$\mathbf{H_{Ee}}$ = [1 0 0 0 ... −1 .... 0] Elevation only

FOR AUTOCOLLIMATOR MOUNT RESPONSE

$\mathbf{H_{AC}}$ = [a0 0 0 0 a1 0 a2 0 a3 0 a4 0 a5 0 .... 0]

NOTES:

All input and output vectors have lengths equal to the dimension of the corresponding linear system matrix, **F**.

The −1 in the Elevation Encoder response is in column $2N + 5$, where N is the number of structure modes modeled.

Coefficients a1. . .a5 are defined as a part of the structure model. When fewer than five structure modes are modeled the a's corresponding to unmodeled modes are replaced with zero and a0 is increased an equal amount such that the sum of a0 + a1 + . . . aN = 1 where N is the number of structure modes modeled.

Table 4. Linear system matrices for closed rate loop

$$F_{CL} = \begin{bmatrix} \begin{bmatrix} & & & & \\ & & F - K_r T & & \\ & & & & \end{bmatrix} & \begin{matrix} 0 & 0 \\ 0 & 0 \\ 0 & 0 \\ 1 & 1 \\ 0 & 0 \\ \cdot & \cdot \\ \cdot & \cdot \\ \cdot & \cdot \end{matrix} \\ \begin{matrix} 0 & 0 & -K_r(Z_2 - P_2) & 0 & \cdots \end{matrix} & \begin{matrix} -P_2 & (Z_2 - P_2) \end{matrix} \\ \begin{matrix} 0 & 0 & -K_r(Z_1 - P_1) & 0 & \cdots \end{matrix} & \begin{matrix} 0 & -P_1 \end{matrix} \end{bmatrix}$$

where T is a matrix with 1.0 in Row 4, Col. 3 and zeros elsewhere

$$G_{CL} = \frac{\omega_m^2}{\nu} \begin{bmatrix} 0 \\ 0 \\ 0 \\ 1 \\ \cdot \\ \cdot \\ \cdot \\ Z_2 - P_2 \\ 0 \end{bmatrix}$$

H_T, H_E, H_{AC} are formed from their open loop counterparts by adding two zero elements following the last element

Table 5. 64- and 70-m antenna structure and servo parameter values

	64-m AZ	70-m AZ	64-m EL	70-m EL
RESIDUAL (Base) INERTIA, J_B	0.1783 (0.2418)	0.1813 (0.2459)	0.0840 (0.1139)	0.1066 (0.1446)
INERTIA Ratio, J_1/J_B	0.3097	0.2356	0.3782	1.1746
INERTIA Ratio, J_2/J_B	0.1092	0.4368	0.3936	0.2383
INERTIA Ratio, J_3/J_B	0.0505	0.2494	0.2729	0.0433
INERTIA Ratio, J_4/J_B	0.0975	0.0436		0.0812
INERTIA Ratio, J_5/J_B		0.0132		0.0121
MOTOR INERTIA, J_M	0.6640 (0.9006)	1.0000 (1.3563)	0.6640 (0.9006)	0.6640 (0.9006)
ALIDADE INERTIA, J_{A1}			0.0145 (0.0197)	0.0145 (0.0197)
ALIDADE INERTIA, J_{A2}			0.1330 (0.1804)	0.1330 (0.1804)
FREQ of $(Kgear/J_B)^{0.5}$	38.3639	38.0399	66.5865	59.1247
FREQ, mode 1, R/s	15.0500	7.9670	19.3830	14.7910
FREQ, mode 2, R/s	25.7600	8.3120	20.7600	17.6930
FREQ, mode 3, R/s	32.0800	9.8900	26.4020	20.2760
FREQ, mode 4, R/s	36.0200	13.7470		21.8340
FREQ, mode 5, R/s		16.9020		25.6290
FREQ of Hyd Motor	9.5940	7.8000	9.5940	9.5940
RE part, Motor freq, D/C	1.2000	1.2000	1.2000	1.2000
FREQ of Alidade 1			67.8258	67.8258
FREQ of Alidade 2			32.0237	32.0237
IRS Transformation coeff. a1	0.1318	0.1331	0.1421	0.2939
a2	0.2022	0.2767	0.1722	0.0977
a3	0.1040	0.1169	0.2090	0.0266
a4	0.0618	0.0099		0.0309
a5		0.0376		0.0050
RATE LOOP GAIN, K_R/ω_m^2	2302	2302	2302	2302
RATE LOOP COMPENSATION NETWORKS, all axes	$\frac{(s+2.2)}{(s+0.12)}$, $\frac{(s+7.1)}{(s+81)}$			

NOTES:

64-m and 70-m azimuth models are for 90 degree elevation.

Inertia values are ft-lb-s^2, (kg-M^2) and are referred to motor shaft.

Natural frequencies are in radians/s.

Coefficient a0 = 1.0000 – a1 – a2 – a3 – a4 – a5.

Table 6a. Transfer functions for 64-m azimuth axis: 3 structure modes modeled

(FILE: AZ6415)	
RESIDUAL (Base) INERTIA, JB	0.1956 (0.2653)
INERTIA Ratio, J1/JB	0.2821
INERTIA Ratio, J2/JB	0.0995
INERTIA Ratio, J3/JB	0.0460
INERTIA Ratio, J4/JB	0.0000
INERTIA Ratio, J5/JB	0.0000
MOTOR INERTIA, JM	0.6640 (0.9006)

OPEN RATE LOOP

VALVE CURRENT TO MOTOR SHAFT TRANSFER FUNCTION

POLES		ZEROS	
Real	Imag	Real	Imag
-5.0933E-003	4.4378E+001	0.0000E+000	4.0634E+001
-5.0933E-003	-4.4378E+001	0.0000E+000	-4.0634E+001
-1.7687E-003	3.1629E+001	0.0000E+000	3.1012E+001
-1.7687E-003	-3.1629E+001	0.0000E+000	-3.1012E+001
-4.2904E-003	2.5545E+001	0.0000E+000	2.4712E+001
-4.2904E-003	-2.5545E+001	0.0000E+000	-2.4712E+001
-2.3554E-002	1.5505E+001	0.0000E+000	1.4625E+001
-2.3554E-002	-1.5505E+001	0.0000E+000	-1.4625E+001
-5.6529E-001	7.8390E+000		
-5.6529E-001	-7.8390E+000		

CLOSED RATE LOOP

RATE LOOP INPUT TO ENCODER RATE TRANSFER FUNCTION

POLES		ZEROS	
Real	Imag	Real	Imag
-3.1927E+000	4.4833E+001		
-3.1927E+000	-4.4833E+001		
-5.5539E-001	3.1564E+001	0.0000E+000	3.2080E+001
-5.5539E-001	-3.1564E+001	0.0000E+000	-3.2080E+001
-8.6159E-001	2.5261E+001	0.0000E+000	2.5760E+001
-8.6159E-001	-2.5261E+001	0.0000E+000	-2.5760E+001
-5.3122E-001	1.4465E+001	0.0000E+000	1.5050E+001
-5.3122E-001	-1.4465E+001	0.0000E+000	-1.5050E+001
-1.2952E+001	1.6448E+001		
-1.2952E+001	-1.6448E+001		
-1.4483E+000	0.0000E+000	-2.2000E+000	0.0000E+000
-4.4686E+001	0.0000E+000	-8.1000E+001	0.0000E+000

CLOSED RATE LOOP

RATE LOOP INPUT TO TACHOMETER RATE TRANSFER FUNCTION

POLES		ZEROS	
Real	Imag	Real	Imag
-3.1927E+000	4.4833E+001	0.0000E+000	4.0634E+001
-3.1927E+000	-4.4833E+001	0.0000E+000	-4.0634E+001
-5.5539E-001	3.1564E+001	0.0000E+000	3.1012E+001
-5.5539E-001	-3.1564E+001	0.0000E+000	-3.1012E+001
-8.6159E-001	2.5261E+001	0.0000E+000	2.4712E+001
-8.6159E-001	-2.5261E+001	0.0000E+000	-2.4712E+001
-5.3122E-001	1.4465E+001	0.0000E+000	1.4625E+001
-5.3122E-001	-1.4465E+001	0.0000E+000	-1.4625E+001
-1.2952E+001	1.6448E+001		
-1.2952E+001	-1.6448E+001		
-1.4483E+000	0.0000E+000	-2.2000E+000	0.0000E+000
-4.4686E+001	0.0000E+000	-8.1000E+001	0.0000E+000

CLOSED RATE LOOP

RATE LOOP INPUT TO AUTOCOLLIMATOR RATE TRANSFER FUNCTION

POLES		ZEROS	
Real	Imag	Real	Imag
-3.1927E+000	4.4833E+001		
-3.1927E+000	-4.4833E+001		
-5.5539E-001	3.1564E+001	0.0000E+000	3.6678E+001
-5.5539E-001	-3.1564E+001	0.0000E+000	-3.6678E+001
-8.6159E-001	2.5261E+001	0.0000E+000	2.8297E+001
-8.6159E-001	-2.5261E+001	0.0000E+000	-2.8297E+001
-5.3122E-001	1.4465E+001	0.0000E+000	1.5985E+001
-5.3122E-001	-1.4465E+001	0.0000E+000	-1.5985E+001
-1.2952E+001	1.6448E+001		
-1.2952E+001	-1.6448E+001		
-1.4483E+000	0.0000E+000	-2.2000E+000	0.0000E+000
-4.4686E+001	0.0000E+000	-8.1000E+001	0.0000E+000

Table 6b. Transfer functions for 70-m azimuth axis: 4 structure modes modeled

(FILE: AZ7028)	
RESIDUAL (Base) INERTIA, JB	0.1837 (0.2492)
INERTIA Ratio, J1/JB	0.2325
INERTIA Ratio, J2/JB	0.4311
INERTIA Ratio, J3/JB	0.2462
INERTIA Ratio, J4/JB	0.0430
INERTIA Ratio, J5/JB	0.0000
MOTOR INERTIA, JM	1.0000 (0.1356)

OPEN RATE LOOP

VALVE CURRENT TO MOTOR SHAFT TRANSFER FUNCTION

POLES		ZEROS	
Real	Imag	Real	Imag
-3.1307E-003	4.2053E+001	0.0000E+000	3.8858E+001
-3.1307E-003	-4.2053E+001	0.0000E+000	-3.8858E+001
-2.8774E-003	1.3785E+001	0.0000E+000	1.3706E+001
-2.8774E-003	-1.3785E+001	0.0000E+000	-1.3706E+001
-6.1942E-002	1.0306E+001	0.0000E+000	9.8101E+000
-6.1942E-002	-1.0306E+001	0.0000E+000	-9.8101E+000
-7.6929E-002	8.9059E+000	0.0000E+000	8.2325E+000
-7.6929E-002	-8.9059E+000	0.0000E+000	-8.2325E+000
-5.9236E-003	8.0631E+000	0.0000E+000	7.9107E+000
-5.9236E-003	-8.0631E+000	0.0000E+000	-7.9107E+000
-4.4911E-001	6.1701E+000		
-4.4911E-001	-6.1701E+000		

CLOSED RATE LOOP

RATE LOOP INPUT TO ENCODER RATE TRANSFER FUNCTION

POLES		ZEROS	
Real	Imag	Real	Imag
-1.5156E+000	4.2566E+001		
-1.5156E+000	-4.2566E+001		
-4.8021E-002	1.3696E+001	0.0000E+000	1.3747E+001
-4.8021E-002	-1.3696E+001	0.0000E+000	-1.3747E+001
-6.7226E-002	9.7472E+000	0.0000E+000	9.8900E+000
-6.7226E-002	-9.7472E+000	0.0000E+000	-9.8900E+000
-3.6465E-002	8.1685E+000	0.0000E+000	8.3120E+000
-3.6465E-002	-8.1685E+000	0.0000E+000	-8.3120E+000
-9.1012E-002	7.8285E+000	0.0000E+000	7.9670E+000
-9.1012E-002	-7.8285E+000	0.0000E+000	-7.9670E+000
-8.4011E+000	1.3145E+001		
-8.4011E+000	-1.3145E+001		
-6.0554E+001	0.0000E+000	-8.1000E+001	0.0000E+000
-1.4472E+000	0.0000E+000	-2.2000E+000	0.0000E+000

CLOSED RATE LOOP

RATE LOOP INPUT TO TACHOMETER RATE TRANSFER FUNCTION

POLES		ZEROS	
Real	Imag	Real	Imag
-1.5156E+000	4.2566E+001	0.0000E+000	3.8858E+001
-1.5156E+000	-4.2566E+001	0.0000E+000	-3.8858E+001
-4.8021E-002	1.3696E+001	0.0000E+000	1.3706E+001
-4.8021E-002	-1.3696E+001	0.0000E+000	-1.3706E+001
-6.7226E-002	9.7472E+000	0.0000E+000	9.8101E+000
-6.7226E-002	-9.7472E+000	0.0000E+000	-9.8101E+000
-3.6465E-002	8.1685E+000	0.0000E+000	8.2325E+000
-3.6465E-002	-8.1685E+000	0.0000E+000	-8.2325E+000
-9.1012E-002	7.8285E+000	0.0000E+000	7.9107E+000
-9.1012E-002	-7.8285E+000	0.0000E+000	-7.9107E+000
-8.4011E+000	1.3145E+001		
-8.4011E+000	-1.3145E+001		
-6.0554E+001	0.0000E+000	-8.1000E+001	0.0000E+000
-1.4472E+000	0.0000E+000	-2.2000E+000	0.0000E+000

CLOSED RATE LOOP

RATE LOOP INPUT TO AUTOCOLLIMATOR RATE TRANSFER FUNCTION

POLES		ZEROS	
Real	Imag	Real	Imag
-1.5156E+000	4.2566E+001		
-1.5156E+000	-4.2566E+001		
-4.8021E-002	1.3696E+001	0.0000E+000	1.3353E+001
-4.8021E-002	-1.3696E+001	0.0000E+000	-1.3353E+001
6.7226E-002	9.7472E+000	0.0000E+000	1.3009E+001
-6.7226E-002	-9.7472E+000	0.0000E+000	-1.3009E+001
-3.6465E-002	8.1685E+000	0.0000E+000	9.2957E+000
-3.6465E-002	-8.1685E+000	0.0000E+000	-9.2957E+000
-9.1012E-002	7.8285E+000	0.0000E+000	8.0628E+000
-9.1012E-002	-7.8285E+000	0.0000E+000	-8.0628E+000
-8.4011E+000	1.3145E+001		
-8.4011E+000	-1.3145E+001		
-6.0554E+001	0.0000E+000	-8.1000E+001	0.0000E+000
-1.4472E+000	0.0000E+000	-2.2000E+000	0.0000E+000

Table 6c. Transfer functions for 64-m elevation axis: 3 tipping structure and 2 alidade modes modeled

(FILE: EL6414)	
RESIDUAL (Base) INERTIA, JB	0.0840 (0.1139)
INERTIA Ratio, J1/JB	0.3782
INERTIA Ratio, J2/JB	0.3936
INERTIA Ratio, J3/JB	0.2729
INERTIA Ratio, J4/JB	0.0000
INERTIA Ratio, J5/JB	0.0000
MOTOR INERTIA, JM	0.6640 (0.9006)

OPEN RATE LOOP

VALVE CURRENT TO MOTOR SHAFT TRANSFER FUNCTION

POLES		ZEROS	
Real	Imag	Real	Imag
-2.2606E-005	1.8661E+002	0.0000E+000	1.8528E+002
-2.2606E-005	-1.8661E+002	0.0000E+000	-1.8528E+002
-5.2814E-004	4.3688E+001	0.0000E+000	4.3309E+001
-5.2814E-004	-4.3688E+001	0.0000E+000	-4.3309E+001
-3.8028E-005	3.1688E+001	0.0000E+000	3.1678E+001
-3.8028E-005	-3.1688E+001	0.0000E+000	-3.1678E+001
-2.9061E-004	2.3835E+001	0.0000E+000	2.3806E+001
-2.9061E-004	-2.3835E+001	0.0000E+000	-2.3806E+001
-1.7055E-004	1.9984E+001	0.0000E+000	1.9976E+001
-1.7055E-004	-1.9984E+001	0.0000E+000	-1.9976E+001
-9.0286E-002	1.4827E+001	0.0000E+000	1.2709E+001
-9.0286E-002	-1.4827E+001	0.0000E+000	-1.2709E+001
-5.0871E-001	8.0624E+000		
-5.0871E-001	-8.0624E+000		

CLOSED RATE LOOP

RATE LOOP INPUT TO ENCODER RATE TRANSFER FUNCTION

POLES		ZEROS	
Real	Imag	Real	Imag
-3.2473E-002	1.8668E+002		
-3.2473E-002	-1.8668E+002		
-2.9969E-001	4.3696E+001	0.0000E+000	4.4681E+001
-2.9969E-001	-4.3696E+001	0.0000E+000	-4.4681E+001
-9.6810E-003	3.1684E+001	0.0000E+000	3.1582E+001
-9.6810E-003	-3.1684E+001	0.0000E+000	-3.1582E+001
-2.2261E-002	2.3809E+001	0.0000E+000	2.3968E+001
-2.2261E-002	-2.3809E+001	0.0000E+000	-2.3968E+001
-4.3576E-003	1.9975E+001	0.0000E+000	1.9799E+001
-4.3576E-003	-1.9975E+001	0.0000E+000	-1.9799E+001
-4.9794E-001	1.2338E+001	0.0000E+000	1.3135E+001
-4.9794E-001	-1.2338E+001	0.0000E+000	-1.3135E+001
-2.0885E+001	1.6166E+001		
-2.0885E+001	-1.6166E+001		
-3.7370E+001	0.0000E+000	-8.1000E+001	0.0000E+000
-1.4486E+000	0.0000E+000	-2.2000E+000	0.0000E+000

CLOSED RATE LOOP

RATE LOOP INPUT TO TACHOMETER RATE TRANSFER FUNCTION

POLES		ZEROS	
Real	Imag	Real	Imag
-3.2473E-002	1.8668E+002	0.0000E+000	1.8528E+002
-3.2473E-002	-1.8668E+002	0.0000E+000	-1.8528E+002
-2.9969E-001	4.3696E+001	0.0000E+000	4.3309E+001
-2.9969E-001	-4.3696E+001	0.0000E+000	-4.3309E+001
-9.6810E-003	3.1684E+001	0.0000E+000	3.1678E+001
-9.6810E-003	-3.1684E+001	0.0000E+000	-3.1678E+001
-2.2261E-002	2.3809E+001	0.0000E+000	2.3806E+001
-2.2261E-002	-2.3809E+001	0.0000E+000	-2.3806E+001
-4.3576E-003	1.9975E+001	0.0000E+000	1.9976E+001
-4.3576E-003	-1.9975E+001	0.0000E+000	-1.9976E+001
-4.9794E-001	1.2338E+001	0.0000E+000	1.2709E+001
-4.9794E-001	-1.2338E+001	0.0000E+000	-1.2709E+001
-2.0885E+001	1.6166E+001		
-2.0885E+001	-1.6166E+001		
-3.7370E+001	0.0000E+000	-8.1000E+001	0.0000E+000
-1.4486E+000	0.0000E+000	-2.2000E+000	0.0000E+000

CLOSED RATE LOOP

RATE LOOP INPUT TO AUTOCOLLIMATOR RATE TRANSFER FUNCTION

POLES		ZEROS	
Real	Imag	Real	Imag
-3.2473E-002	1.8668E+002		
-3.2473E-002	-1.8668E+002		
-2.9969E-001	4.3696E+001	0.0000E+000	7.2267E+001
-2.9969E-001	-4.3696E+001	0.0000E+000	-7.2267E+001
-9.6810E-003	3.1684E+001	0.0000E+000	3.4188E+001
-9.6810E-003	-3.1684E+001	0.0000E+000	-3.4188E+001
-2.2261E-002	2.3809E+001	0.0000E+000	3.0055E+001
-2.2261E-002	-2.3809E+001	0.0000E+000	-3.0055E+001
-4.3576E-003	1.9975E+001	0.0000E+000	2.2681E+001
-4.3576E-003	-1.9975E+001	0.0000E+000	-2.2681E+001
-4.9794E-001	1.2338E+001	0.0000E+000	1.9844E+001
-4.9794E-001	-1.2338E+001	0.0000E+000	-1.9844E+001
-2.0885E+001	1.6166E+001		
-2.0885E+001	-1.6166E+001		
-3.7370E+001	0.0000E+000	-8.1000E+001	0.0000E+000
-1.4486E+000	0.0000E+000	-2.2000E+000	0.0000E+000

Table 6d. Transfer functions for 70-m elevation axis: 3 tipping structure and 2 alidade modes modeled

INERTIA AND FREQ OF 3rd MODE ARE ADJUSTED COMPOSITES OF MODES 3, 4, 5

(FILE: EL7012)	
RESIDUAL (Base) INERTIA, JB	0.1066 (0.1446)
INERTIA Ratio, J1/JB	1.1746
INERTIA Ratio, J2/JB	0.2383
INERTIA Ratio, J3/JB	0.1362
FREQ, mode 3, R/s	21.7400
INERTIA Ratio, J4/JB	0.0000
INERTIA Ratio, J5/JB	0.0000
MOTOR INERTIA, JM	0.6640 (0.9006)

OPEN RATE LOOP

VALVE CURRENT TO MOTOR SHAFT TRANSFER FUNCTION

POLES		ZEROS	
Real	Imag	Real	Imag
-2.3597E-005	1.8433E+002	0.0000E+000	1.8299E+002
-2.3597E-005	-1.8433E+002	0.0000E+000	-1.8299E+002
-6.7820E-004	4.1970E+001	0.0000E+000	4.1540E+001
-6.7820E-004	-4.1970E+001	0.0000E+000	-4.1540E+001
-1.3184E-004	2.7651E+001	0.0000E+000	2.7629E+001
-1.3184E-004	-2.7651E+001	0.0000E+000	-2.7629E+001
-7.1847E-004	2.0753E+001	0.0000E+000	2.0711E+001
-7.1847E-004	-2.0753E+001	0.0000E+000	-2.0711E+001
-1.8263E-003	1.7085E+001	0.0000E+000	1.7039E+001
-1.8263E-003	-1.7085E+001	0.0000E+000	-1.7039E+001
-1.8590E-001	1.2952E+001	0.0000E+000	9.8583E+000
-1.8509E-001	-1.2952E+001	0.0000E+000	-9.8583E+000
-4.1066E-001	7.1233E+000		
-4.1066E-001	-7.1233E+000		

CLOSED RATE LOOP

RATE LOOP INPUT TO ENCODER RATE TRANSFER FUNCTION

POLES		ZEROS	
Real	Imag	Real	Imag
-3.3846E-002	1.8441E+002		
-3.3846E-002	-1.8441E+002		
-3.5693E-001	4.1960E+001	0.0000E+000	4.2889E+001
-3.5693E-001	-4.1960E+001	0.0000E+000	-4.2889E+001
-2.0608E-002	2.7636E+001	0.0000E+000	2.7644E+001
-2.0608E-002	-2.7636E+001	0.0000E+000	-2.7644E+001
-2.5872E-002	2.0708E+001	0.0000E+000	2.0737E+001
-2.5872E-002	-20.708E+001	0.0000E+000	-2.0737E+001
-1.5653E-002	1.7033E+001	0.0000E+000	1.7050E+001
-1.5653E-002	-1.7033E+001	0.0000E+000	-1.7050E+001
-3.2123E-001	9.4835E+000	0.0000E+000	1.0185E+001
-3.2123E-001	-9.4835E+000	0.0000E+000	1.0185E+001
-2.0812E+001	1.6437E+001		
-2.0812E+001	-1.6437E+001		
-3.7699E+001	0.0000E+000	-8.1000E+001	0.0000E+000
-1.4483E+000	0.0000E+000	-2.2000E+000	0.0000E+000

CLOSED RATE LOOP

RATE LOOP INPUT TO TACHOMETER RATE TRANSFER FUNCTION

POLES		ZEROS	
Real	Imag	Real	Imag
-3.3846E-002	1.8441E+002	0.0000E+000	1.8299E+002
-3.3846E-002	-1.8441E+002	0.0000E+000	-1.8299E+002
-3.5693E-001	4.1960E+001	0.0000E+000	4.1540E+001
-3.5693E-001	-4.1960E+001	0.0000E+000	-4.1540E+001
-2.0608E-002	2.7636E+001	0.0000E+000	2.7629E+001
-2.0608E-002	-2.7636E+001	0.0000E+000	-2.7629E+001
-2.5872E-002	2.0708E+001	0.0000E+000	2.0711E+001
-2.5872E-002	-2.0708E+001	0.0000E+000	-2.0711E+001
-1.5653E-002	1.7033E+001	0.0000E+000	1.7039E+001
-1.5653E-002	-1.7033E+001	0.0000E+000	-1.7039E+001
-3.2123E-001	9.4835E+000	0.0000E+000	9.8583E+000
-3.2123E-001	-9.4835E+000	0.0000E+000	-9.8583E+000
-2.0812E+001	1.6437E+001		
-2.0812E+001	-1.6437E+001		
-3.7699E+001	0.0000E+000	-8.1000E+001	0.0000E+000
-1.4483E+000	0.0000E+000	-2.2000E+000	0.0000E+000

CLOSED RATE LOOP

RATE LOOP INPUT TO AUTOCOLLIMATOR RATE TRANSFER FUNCTION

POLES		ZEROS	
Real	Imag	Real	Imag
-3.3846E-002	1.8441E+002		
-3.3846E-002	-1.8441E+002		
-3.5693E-001	4.1960E+001	0.0000E+000	7.2267E+001
-3.5693E-001	-4.1960E+001	0.0000E+000	-7.2267E+001
-2.0608E-002	2.7636E+001	0.0000E+000	3.0055E+001
-2.0608E-002	-2.7636E+001	0.0000E+000	-3.0055E+001
-2.5872E-002	2.0708E+001	0.0000E+000	2.2960E+001
-2.5872E-002	-2.0708E+001	0.0000E+000	-2.2960E+001
-1.5653E-002	1.7033E+001	0.0000E+000	1.9858E+001
-1.5653E-002	-1.7033E+001	0.0000E+000	-1.9858E+001
-3.2123E-001	9.4835E+000	0.0000E+000	1.6359E+001
-3.2123E-001	-9.4835E+000	0.0000E+000	-1.6359E+001
-2.0812E+001	1.6437E+001		
-2.0812E+001	-1.6437E+001		
-3.7699E+001	0.0000E+000	-8.1000E+001	0.0000E+000
-1.4483E+000	0.0000E+000	-2.2000E+000	0.0000E+000

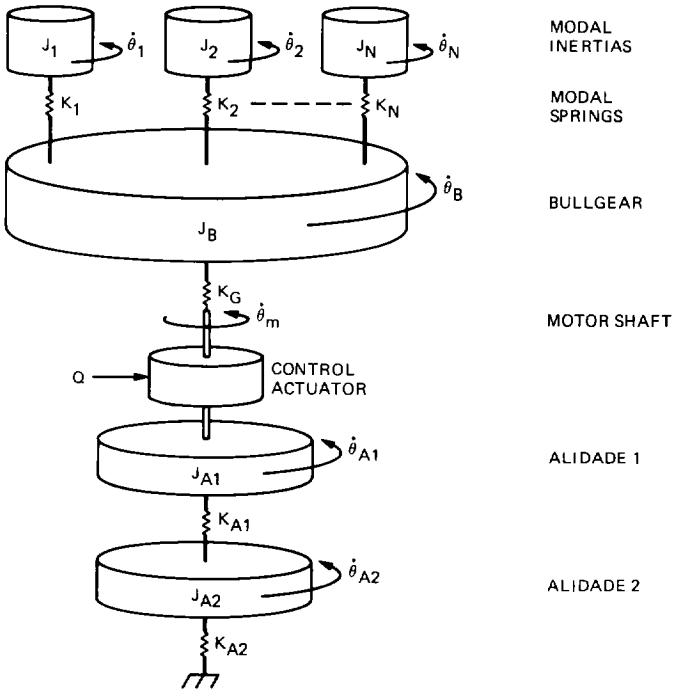

Fig. 1. Structure model schematic representation

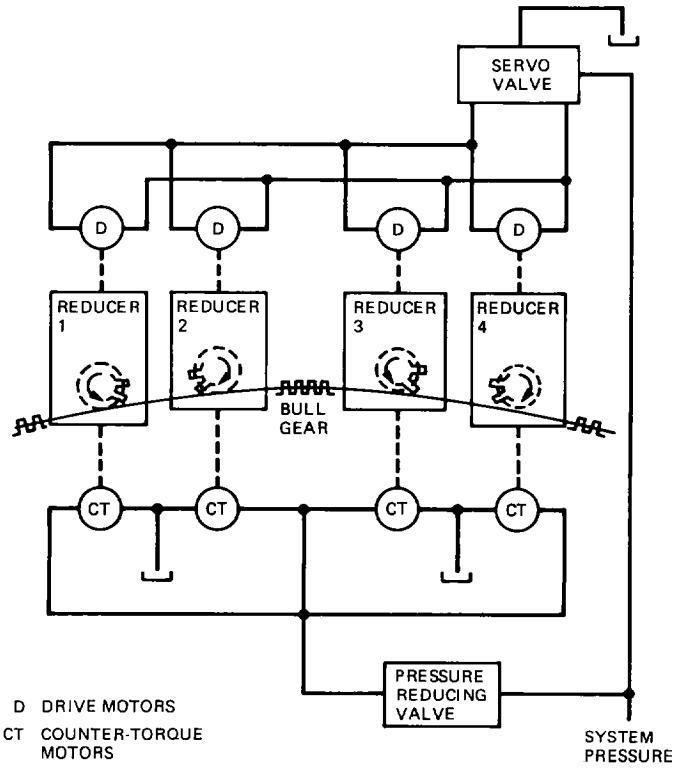

Fig. 2. Countertorque system, 64/70-m antenna

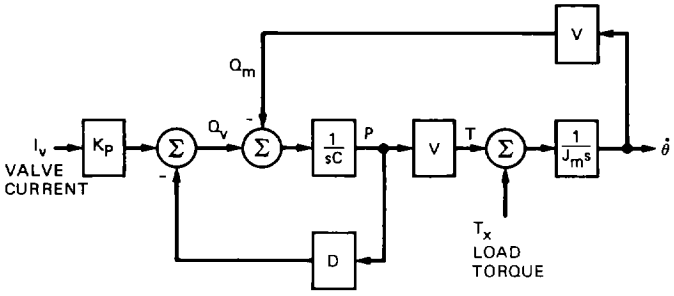

Fig. 3. Hydraulic motor linearized block diagram

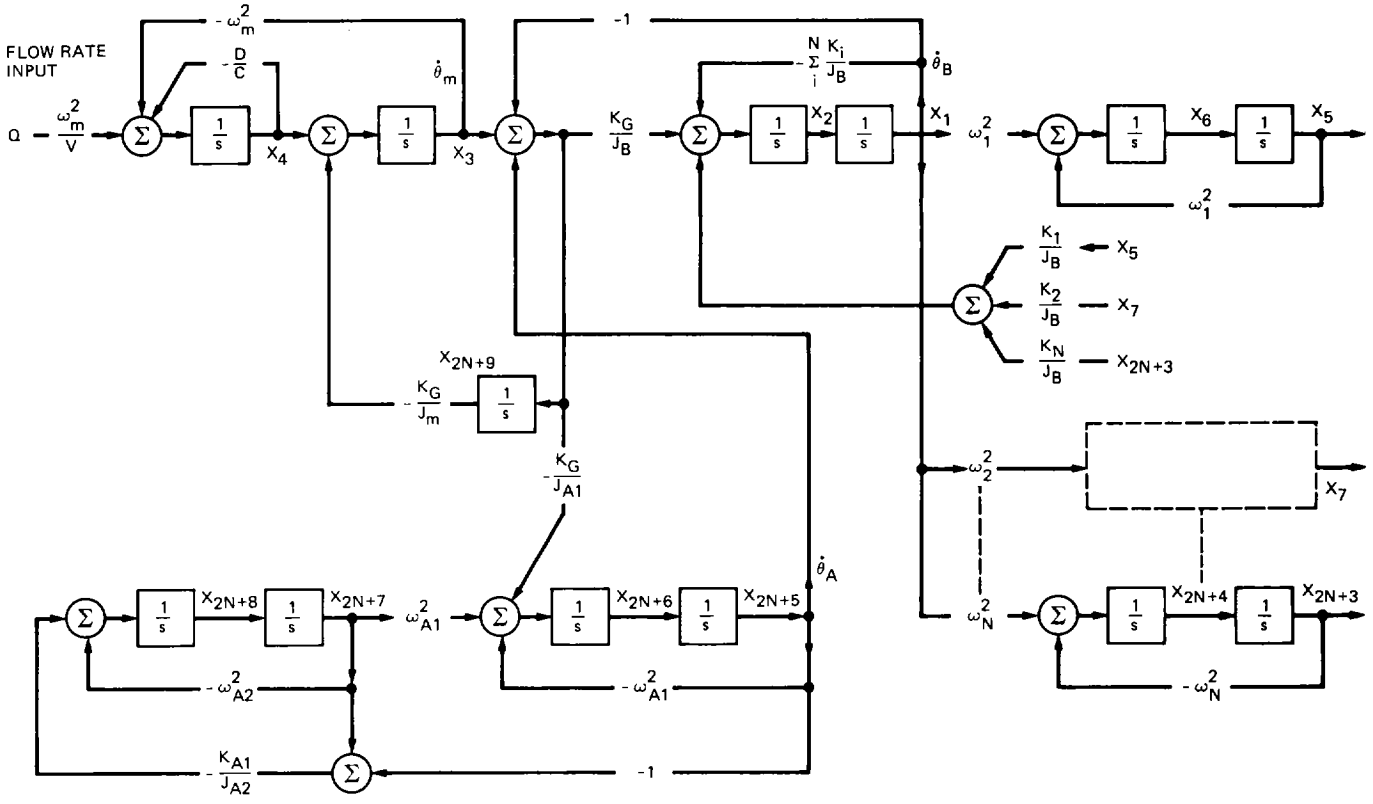

Fig. 4. Elevation open loop system block diagram

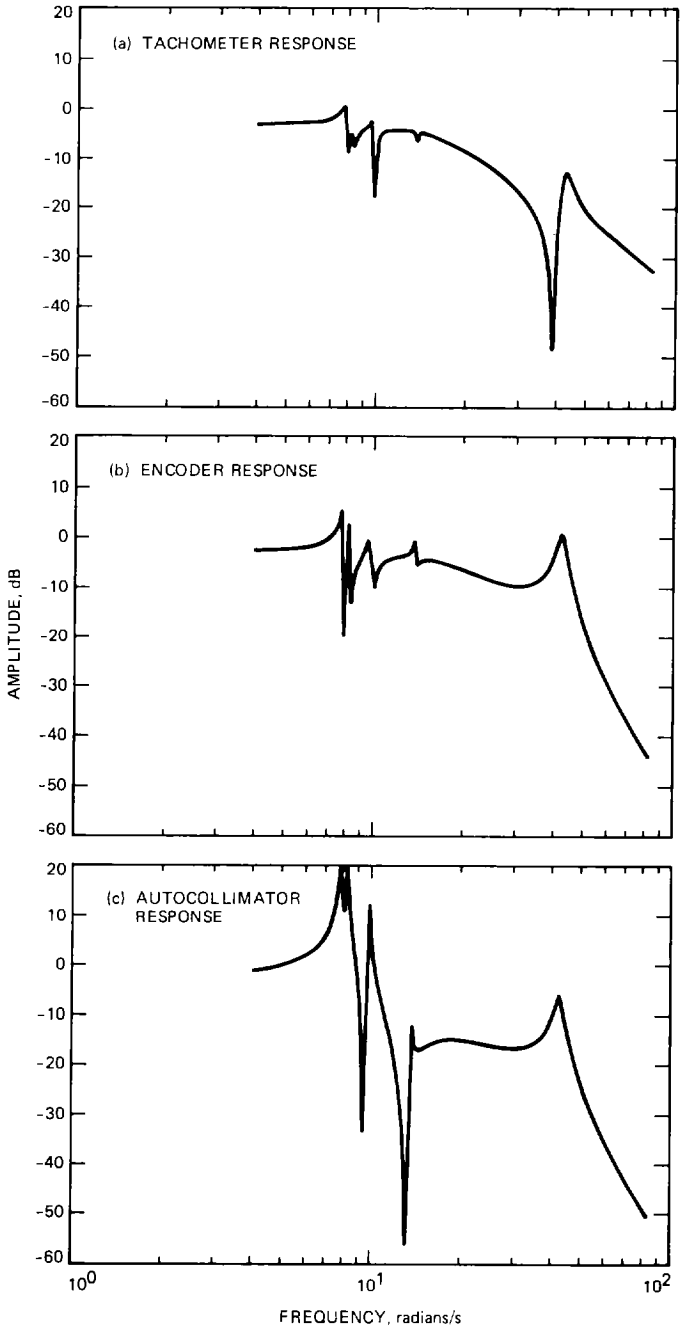

Fig. 5. Amplitude response vs. frequency for 70-m azimuth

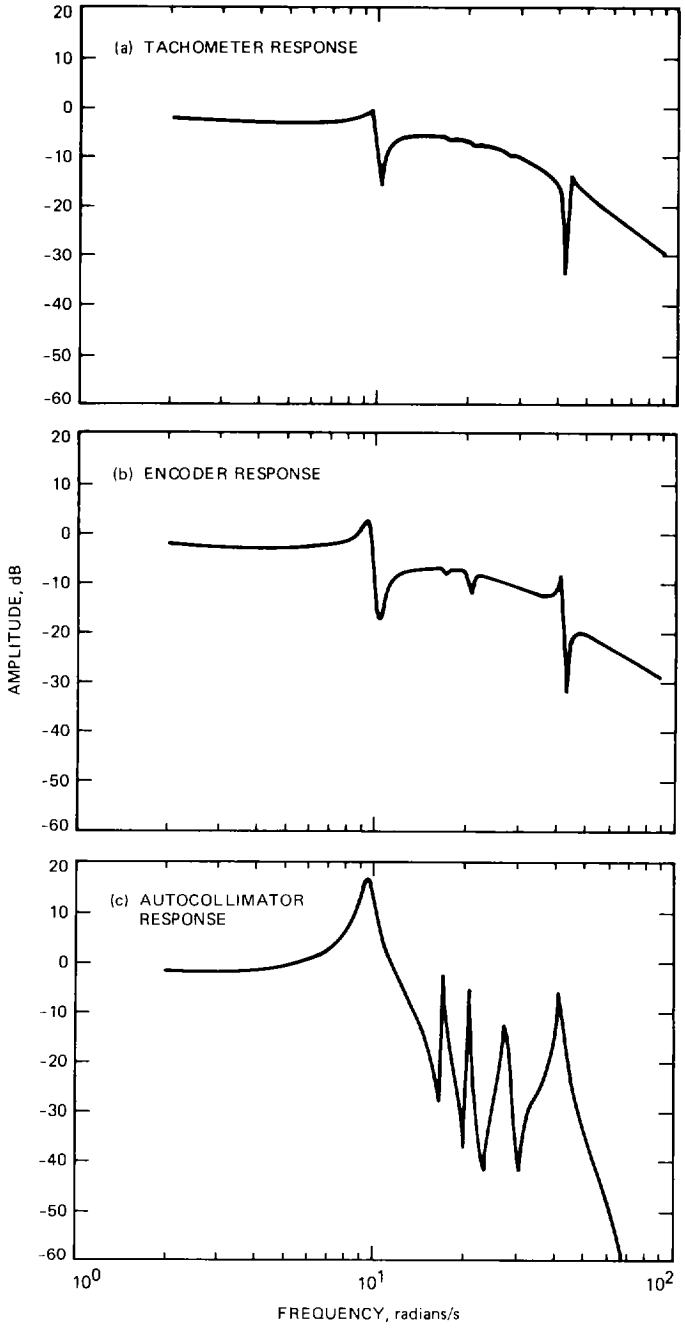

Fig. 6. Elevation response vs. frequency, 70-m antenna